SCIENTIFIC REPORTS

OPEN

SUBJECT AREAS:
MICROFLUIDICS
CHARACTERIZATION AND ANALYTICAL TECHNIQUES
PROTEIN ANALYSIS

Received
17 October 2013

Accepted
19 December 2013

Published
16 January 2014

Correspondence and requests for materials should be addressed to M.J.A.S. (m.shiddiky@uq.edu.au) or M.T. (m.trau@uq.edu.au)

Molecular *Nanoshearing*: An Innovative Approach to Shear off Molecules with AC-Induced Nanoscopic Fluid Flow

Muhammad J. A. Shiddiky[1], Ramanathan Vaidyanathan[1], Sakandar Rauf[1], Zhikai Tay[1] & Matt Trau[1,2]

[1]Australian Institute for Bioengineering and Nanotechnology (AIBN), Corner College and Cooper Roads (Bldg 75), The University of Queensland, Brisbane QLD 4072, Australia, [2]School of Chemistry and Molecular Biosciences, The University of Queensland, Brisbane, QLD 4072, Australia.

Early diagnosis of disease requires highly specific measurement of molecular biomarkers from femto to pico-molar concentrations in complex biological (*e.g.*, serum, blood, etc.) samples to provide clinically useful information. While reaching this detection limit is challenging in itself, these samples contain numerous other non-target molecules, most of which have a tendency to adhere to solid surfaces *via* nonspecific interactions. Herein, we present an entirely new methodology to physically displace nonspecifically bound molecules from solid surfaces by utilizing a newly discovered "*tuneable force*", induced by an applied alternating electric field, which occurs within few nanometers of an electrode surface. This methodology thus offers a unique ability to shear-off loosely bound molecules from the solid/liquid interface. Via this approach, we achieved a 5-fold reduction in nonspecific adsorption of non-target protein molecules and a 1000-fold enhancement for the specific capture of HER2 protein in human serum.

Nonspecific adsorption of molecules has been a major limitation of existing molecular detection methodologies, particularly for protein detection in biological and clinical samples[1,2], where target molecules are often present at concentrations many orders of magnitude lower than non-target molecules. These non-target molecules have a tendency to adhere nonspecifically to sensor surfaces thereby significantly reducing specificity and sensitivity[3,4], and is also a major problem in other fields as diverse as biomedical device implants[5] and marine fouling on the hull of ships[6]. This long-standing problem has been commonly addressed by a multitude of approaches that chemically modify the surface with "non-fouling" molecular coatings such as polyethylene glycol[7] and zwitterions complexes[8]. Furthermore, microfluidic devices that rely primarily on diffusive mixing are generally associated with nonspecific adsorption of proteins owing to longer mixing periods[9,10]. Herein, we describe an entirely new approach which enables the physical displacement of weakly (nonspecifically) bound molecules using a *tuneable* alternating current electrohydrodynamic (ac-EHD) force, referred to as *"nanoshearing"*.

Nanoshearing is an ac-EHD induced phenomenon that engenders fluid flow due to electrical body forces generated within few nanometers of an aqueous electrolyte/electrode interface. Upon application of an alternating potential difference across large and small microelectrodes in an asymmetric electrode pair, a non-uniform field ($\boldsymbol{E}$) induces charges within the electrical double layer (Fig. 1a, b) near the electrode surface. The asymmetric geometry of the electrodes give rise to a lateral variation in the total amount of induced (double layer) charges and spatial distribution of charges on the electrode surface. Consequently, the induced charges on the larger electrode experience stronger lateral forces than those on the smaller electrode ($\boldsymbol{F}_L > \boldsymbol{F}_s$, where $\boldsymbol{F}_L$ and $\boldsymbol{F}_s$ are the resultant forces generated on large and small electrodes, respectively, due to interaction with the tangential component of the applied ac field), resulting in a lateral flow towards the large electrode[11,12]. One special feature of this flow is that because the induced charges in the interface occur only within the double layer of the electrode, all of the EHD forces on the fluid also occur strictly within this region. The characteristic thickness of the double layer is given by the Debye length[13], λ_D ($=1/\kappa$), which can be calculated based on the following equation:

$$\kappa = \left(\frac{2000F^2}{\varepsilon_0 \varepsilon_r kT}\right)^{\frac{1}{2}} \sqrt{I} \quad \text{in units of } \mathrm{m}^{-1} \tag{1}$$

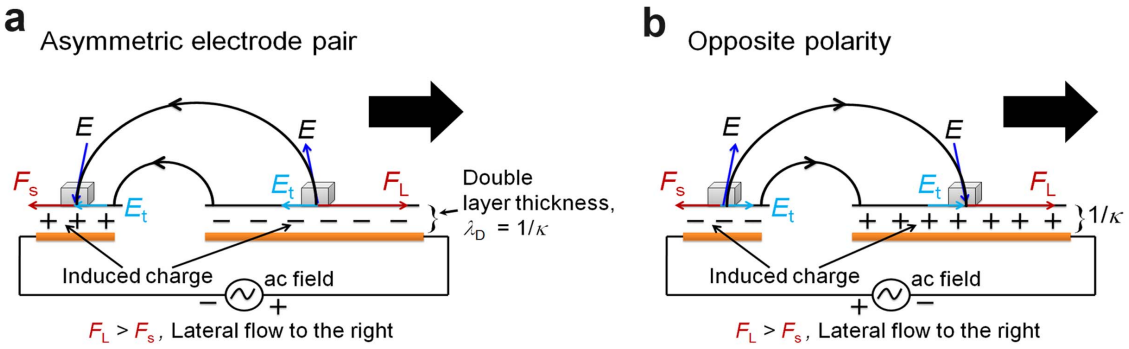

Figure 1 | Mechanism of ac-EHD induced fluid flow. (a) Upon application of ***E***, the induced charges in the double layer of each electrode experience a force ***F*** ($\boldsymbol{F}=\rho\boldsymbol{E}_t$, where ρ=charge density) and produce a net fluid flow in the direction of the broken symmetry. (b) Reversing the polarity of the ac field also reverses the sign of the charges in the induced double layer, and since electrical body forces are the product of the charges and the applied field, a steady flow can be maintained towards the large electrode.

$$= 3.288\sqrt{I}\,(\mathrm{nm}^{-1}) \qquad (2)$$

where, $^1/_\kappa$= double layer thickness, F is faraday constant, I = ionic strength = ½ $\Sigma c_i z_i^2$ (c_i = ionic concentration in molL^{-1}, z_i = valency). In our case, these forces engender shear flow within few nanometers from the electrode surface (*e.g.*, λ_D=1.2 nm for 10 mM phosphate buffered saline (PBS) solution with the conductivity of Λ=~15.4 mSm^{-1} at 25°C) and give rise to complex fluid mixing near the electrode.

Results and Discussion

To investigate the *nanoshearing* phenomenon, two purpose-built microfluidic devices (see Methods for design and fabrication details) were constructed: **Device 1** (Supplementary Fig. S1a) contains a long array of consecutively placed asymmetric electrode pairs within a serpentine microchannel (Supplementary Fig. S2a for fabrication), while **Device 2** (Supplementary Fig. S1b) composed of asymmetric electrode pairs with a combination of planar and microtip spikes (Supplementary Fig. S2b for fabrication). When the devices were filled with an aqueous buffer solution, ac-EHD field engenders a left-to-right unidirectional flow. To check the fluid flow patterns in these devices, fluorescent latex particles (970 nm diameter) were used. Under ac-EHD field, unidirectional flow (velocity =30±3 $\mu\mathrm{ms}^{-1}$) was observed with the particles travelling from the smaller to larger electrode in **Device 1** (Supplementary Fig. S3, movie 1) and no particle movement was observed in the absence of ac field (Supplementary Fig. S3, movie 2). Similar fluid flow observations have previously been demonstrated using coplanar electrodes[14] and an array of asymmetric electrode pairs[11,12] that produce steady fluid flow under nonuniform ac fields[15,16]. We then incorporated microtips to further induce spatial asymmetry in the device geometry (*e.g.*, **Device 2**). As can be seen in video 3 in Supplementary Fig. S4, the particle flow pattern in **Device 2**, which used the microtip electrodes, demonstrated micromixing of particles with particles travelling from the inlet to the outlet of the device (video 4 in Supplementary Fig. S4 is for the control device in the absence of ac field). It is predicted that the presence of microtips accentuate the surface shear forces and concomitant micromixing effect *via*: (*i*) increased surface area, (*ii*) more complex and asymmetric electric field lines, and (*iii*) greater complexity of fluid flow.

To demonstrate the use of *nanoshearing* effect for molecular target detection, we tested the capture and detection of human epidermal growth factor receptor 2 (HER2) antigen spiked into PBS or human serum. The samples were run on anti-HER2 functionalized (see Methods for details) devices (Supplementary Fig. S5) under the frequency (f) range of 600 Hz-100 kHz at constant amplitude (V_{pp}) of 100 mV. Figures 2a, b are schematic representations and Supplementary Fig. S6 contains 3D animations (movies 5 and 6) demonstrating *nanoshearing* effect for protein capture. Panels (a) and (b) in Fig. 3 provide typical fluorescence image analysis (see Methods for detailed analysis procedure) obtained using **Device 1** and **2** for 100 pgmL^{-1} HER2 antigen spiked in PBS under the frequency of 600 Hz and 100 kHz at V_{pp}=100 mV. Capture performance for both devices operating at a frequency of 600 Hz was found to be significantly increased (2-fold for **Device 1** and 3-fold in **Device 2**) in comparison to that of 100 kHz. These data indicate that the capture performance of our devices is a function of applied field strength. The resulting high level of capture at low field strength is probably due to the stimulation of the fluid flow around the anti-HER2 functionalized electrodes, which can maximize the effective protein-antibody collisions (a condition where shear force < antibody-antigen binding force). In contrast, at high field strength (*e.g.*, f=100 kHz, V_{pp}=100 mV) protein-antibody impact does not occur effectively due to the stronger fluid flow (a condition where shear forces > antibody-antigen affinity interaction), which could ablate HER2 antigen recognition and decrease the capture level. The microtips in **Device 2** (Supplementary Fig. S7, movie 7) provide high aspect ratio structures with additional surface area and disrupt the streamlines to induce better fluid mixing thereby increasing the number of antibody-antigen interactions which leads to increased capture performance. Therefore, the low field strength (*e.g.*, f=1 kHz, V_{pp}=100 mV) was used for further studies in demonstrating the application of ac-EHD induced *nanoshearing* phenomenon for the detection of proteins.

Control experiments to compare the capture performance of the devices under ac-EHD flow to that of a hydrodynamic flow was performed using a pressure-driven system (*via* a syringe pump) to drive fluid through the devices with the similar flow rate. Fluorescence image analysis data for the capture of 100 pgmL^{-1} HER2 under hydrodynamic flow condition are represented in Fig. 3. Under the ac-EHD field conditions, the devices yielded a 2 (**Device 1**) and 6-fold (**Device 2**) higher capture yields in comparison with the devices operating under hydrodynamic flow conditions. This high capture yield is presumably owing to the ac-EHD induced fluid flow and manipulation of the shear forces within the double layer, which could maximize the effective antibody-antigen affinity interaction.

To validate the specificity and accuracy of the immunocapture, control experiments were performed using serum samples spiked with (100 pgmL^{-1}) and without HER2. Under the field strength of f=1 kHz and V_{pp}=100 mV, negligible nonspecific binding of the detection antibody was observed in both ac-EHD (dark-gray *versus* red bars in Fig. 4a, b) devices. Furthermore, approximately 2.5 (**Device 1**) and 5-fold (**Device 2**) enhancement in the detection capabilities was observed under ac-EHD in comparison to the hydrodynamic flow based control devices. To investigate the effect of BSA

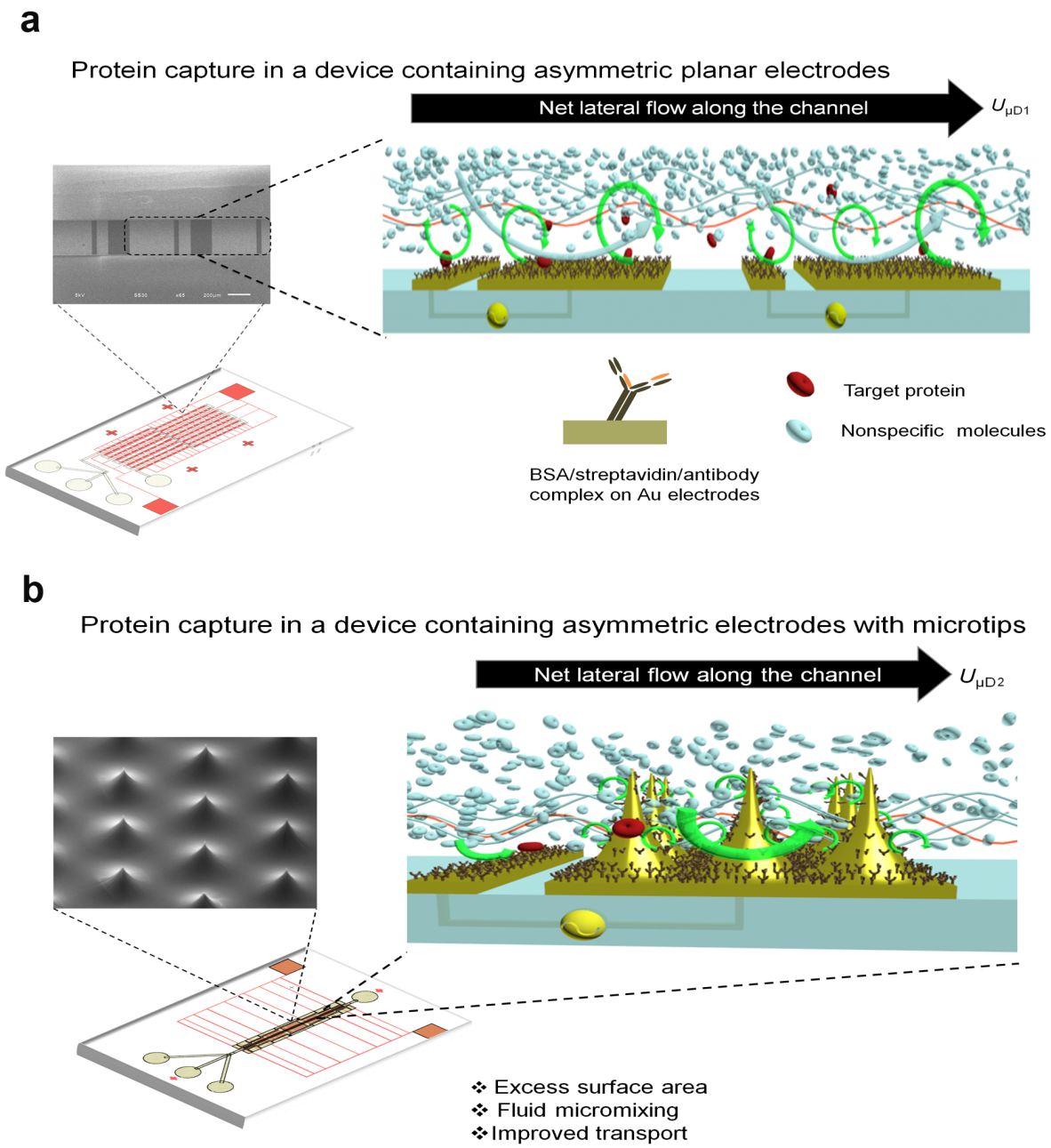

Figure 2 | ac-EHD induced *nanoshearing*. (a) In **Device 1**, a unidirectional fluid flow, $U_{\mu D1}$, occurs along the channel (*e.g.*, towards the larger electrode in the pairs). This ac-EHD induced fluid flow generates micro- and nanoscopic shear forces within the double layer (*e.g.*, *nanoshearing*), which can shear away nonspecifically adsorbed molecules. (b) In **Device 2**, the presence of the additional spikes on the larger electrodes, create more complex field lines, and thus, fluid exhibits complex flow movements. Arrow indicates the direction of objects moving along the fluid under ac-EHD field.

blocking on detection capabilities of the devices, we performed additional control experiments using BSA blocked anti-HER2 functionalized devices. Serum samples without HER2 antigens were driven through the devices under both ac-EHD and hydrodynamic flow conditions. As can be seen in Fig. 4a, b (inset), BSA blocking did not have a substantial effect in altering detection capabilities of the devices (similar nonspecific binding of the detection antibody) in comparison to the devices without BSA blocking. Representative fluorescence images of the detected HER2 protein and nonspecifically bound antibody are shown in Supplementary Fig. S8a, b. This data suggests that ac-EHD induced *nanoshearing* can enhance the detection capabilities of the devices by enhancing the specificity of capture and accuracy of the immunoassay.

To demonstrate the utility of the *nanoshearing* phenomena in removing nonspecific proteins present in serum samples, HER2 (500 pgmL^{-1}) along with nonspecific IgG (500 pgmL^{-1}) protein were spiked in serum and run on anti-HER2-functionalized devices. Under the ac field of f=1 kHz and V_{pp}=100 mV, the capture performance was evaluated using **Device 2**. An approximately 5-fold reduction (Fig. 5a) in the number of nonspecific proteins that adhere to the electrode surface in comparison to the pressure-driven flow based device was observed. Representative fluorescence images of detected HER2 and IgG protein are shown in Fig. 5b, c. This data clearly demonstrates that *nanoshearing* phenomenon is highly effective in reducing nonspecific adsorption of proteins in comparison with pressure driven flow based approach.

To further assess the dynamic range and lower limit of detection (LOD) of our devices, designated concentrations of HER2 (100 pgmL^{-1} to 1 fgmL^{-1}) were spiked in serum and run on anti-HER2-functionalized devices under the optimal ac field strength of

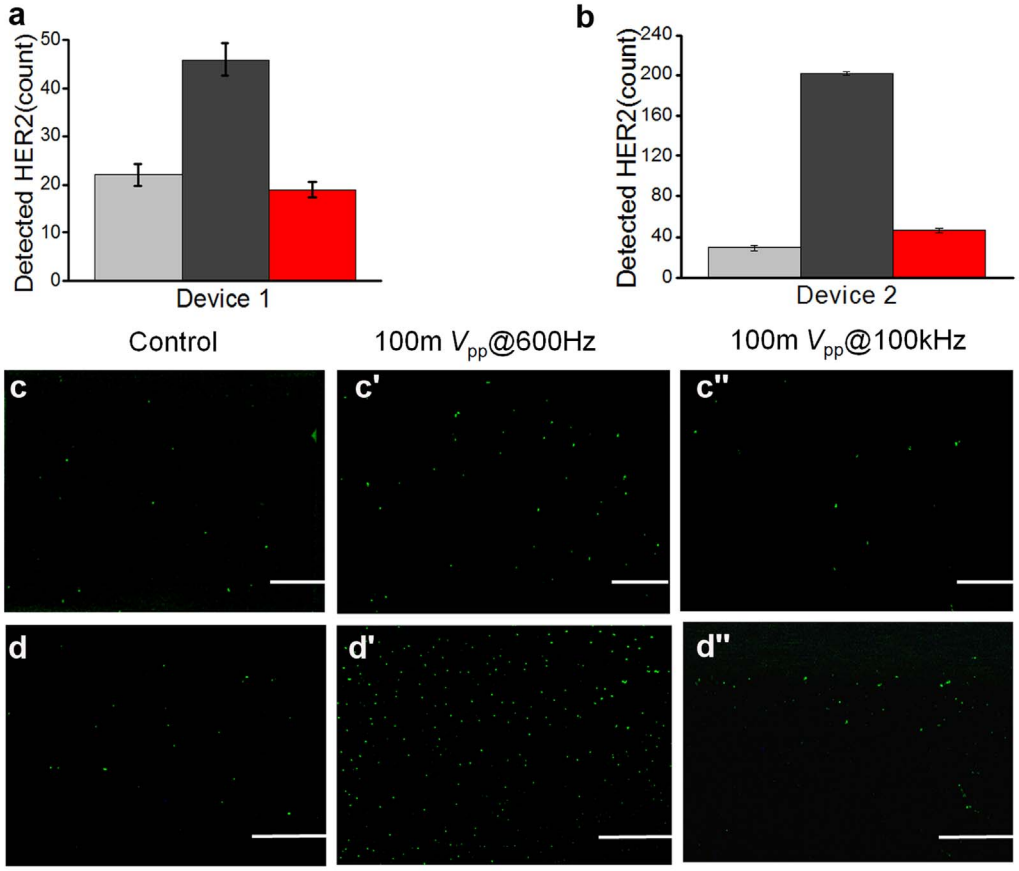

Figure 3 | Fluorescence imaging of the captured HER2 protein at different ac field conditions. (a,b) Fluorescence image analysis of HER2 (100 pgmL^{-1} spiked in PBS) capture at the frequency of f=600 Hz (dark gray) and 100 kHz (red) at V_{pp}=100 mV in (a) **Device 1** and (b) **Device 2**. Control devices (light gray) include those tested under pressure driven flow conditions. Pressure driven flow based devices operated under the rate of 10 μLmin^{-1} (an equivalent flow rate of that calculated based on the time required to flow 1 mL of sample under the given ac-EHD field). Each data point represents the average of three separate trials *(n=3)* and error bars represent standard error of measurements within each experiment. (c,d) Representative fluorescence images of the detected HER2 protein in (c,c′,c″) **Device 1** and (d,d′,d″) **Device 2**. Scale bar is 100 μm. The optimal ac-EHD conditions for **Device 1** and **2** was determined to be 1 kHz at 100 mV.

f=1 kHz and V_{pp}=100 mV. Control experiments were performed with that of a pressure driven system to drive fluid through the devices at similar flow-rate (see Methods for details). Under ac-EHD field, fluorescence image analysis for **Device 1** and **2** suggested approximately 10 (Fig. 6a; 100 fgmL^{-1} (ac-EHD) *vs.* 1 pgmL^{-1} (control) for **Device 1**) and 1000 fold (Fig. 6b; 1 fgmL^{-1} (ac-EHD) *vs.* 1 pgmL^{-1} (control) for **Device 2**) increase in detection levels in comparison to the control devices. The linear dynamic range of detection for **Device 1** and **Device 2** was found to be 100 fgmL^{-1}-100 pgmL^{-1} and 1 fgmL^{-1}-100 pgmL^{-1}, respectively. Representative

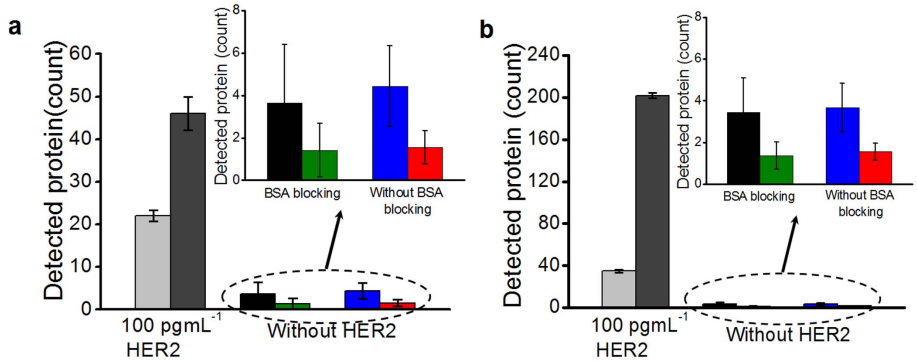

Figure 4 | Specificity and accuracy of immunocapture. (a,b) Fluorescence image analysis of proteins from human serum spiked with (100 pgmL^{-1}; light gray (control), dark gray (ac-EHD)) and without HER2 under ac-EHD (f=1 kHz, V_{pp}=100 mV) and pressure driven (control) flow condition in (a) **Device 1** and (b) **Device 2**. Inset shows fluorescence image analysis of proteins from human serum without HER2 on anti-HER2-functionalized devices blocked with (black, control; green, ac-EHD) and without (blue, control; red, ac-EHD) BSA. Pressure driven flow based devices operated under the rate of 10 μLmin^{-1} (an equivalent flow rate of that calculated based on the time required to flow 1 mL of serum samples under the given ac-EHD field). Each data point represents the average of three separate trials *(n=3)* and error bars represent standard error of measurements within each experiment.

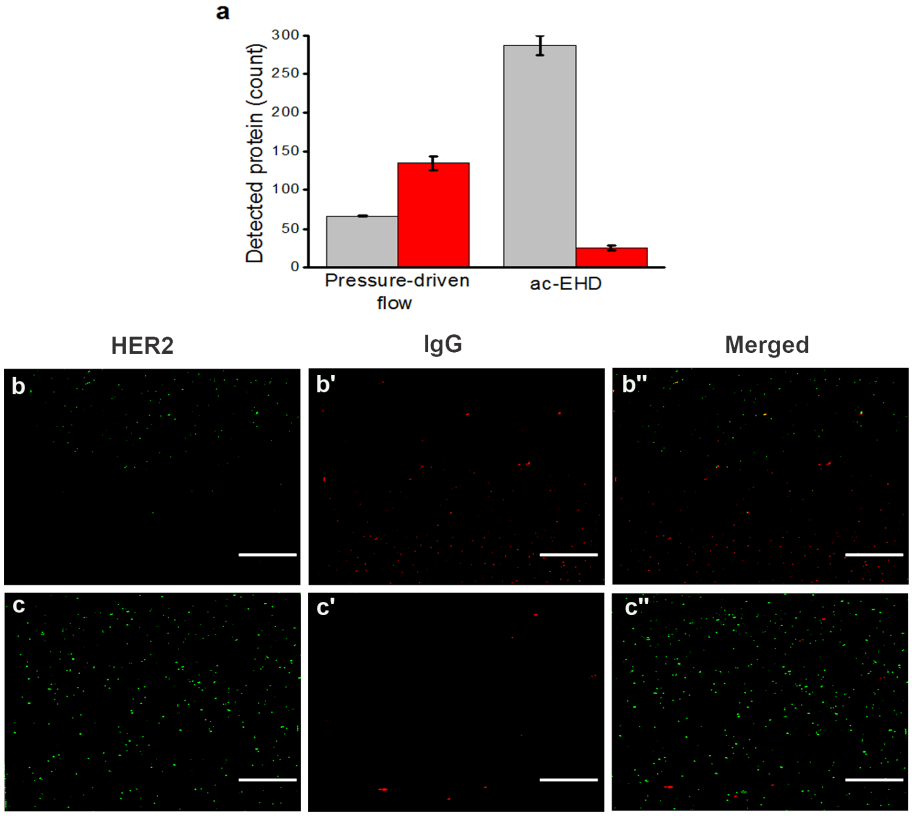

Figure 5 | ac-EHD induced *nanoshearing* effect on nonspecific adsorption of proteins. (a) Fluorescence image analysis of the detected HER2 protein (gray) spiked in human serum along with mouse IgG (red) was run on **Device 2** under ac-EHD (f=1 kHz, V_{pp}=100 mV) and pressure-driven flow (control) conditions. Pressure driven flow based devices operated under the rate of 10 μLmin^{-1} (an equivalent flow rate of that calculated based on the time required to flow 1 mL of serum sample under the given ac-EHD field). Each data point represents the average of three separate trials (n=3) and error bars represent standard error of measurements within each experiment. (b,c) Representative images for captured HER2 (green) and nonspecifically bound IgG (red) proteins under ac-EHD (c,c′,c″) and pressure driven (b,b′,b″) flow conditions. Scale bar is 100 μm.

images of HER2 capture at designated concentrations in these devices are shown in Supplementary Fig. S9. The enhanced HER2 capture with the use of ac-EHD induced fluid flow compared to the pressure driven flow based devices may be attributed to the synergistic effect of using a specific HER2 antibody, geometric arrangements of the antibody-functionalized microelectrode pairs within the channel, ac-EHD induced *nanoshearing* and concomitant fluid mixing phenomena. It is clearly noted that **Device 2** (Fig. 6b) was sensitive enough to detect 1 fgmL^{-1} HER2 antigen spiked in serum samples, while the minimum detectable concentration for **Device 1** was 100 fgmL^{-1} (Fig. 6a). The LOD values obtained in serum samples indicate that our method can be used to detect low concentrations of molecular targets in complex fluids. To further examine the effect of *nanoshearing* and concomitant fluid mixing to capture low concentration of target proteins in large excess of non-target proteins, we spiked two nonspecific proteins CA-125 (100 pgmL^{-1}) and PSA (100 pgmL^{-1}) in serum along with HER2 (1 fgmL^{-1}) and the effect was evaluated. As can be seen in Supplementary Fig. S10, **Device 2** was sensitive enough to detect 1 fgmL^{-1} HER2 indicating that this device can detect low concentration of target proteins in the

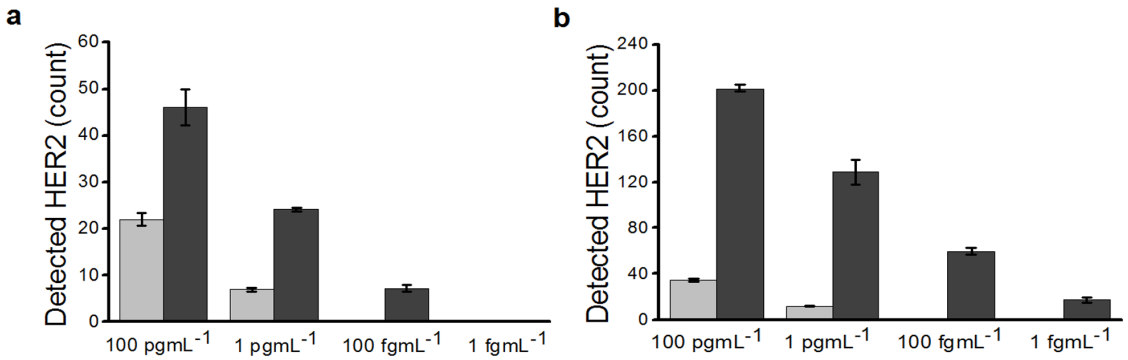

Figure 6 | ac-EHD induced *nanoshearing* for HER2 capture. (a,b) Fluorescence image analysis of the detected HER2 protein (100 pgmL^{-1} to 1 fgmL^{-1}) spiked in human serum under ac-EHD (f=1 kHz, V_{pp}=100 mV; dark gray bar) and pressure driven flow (control; light gray bar) conditions in (a) **Device 1** and (b) **2**. Pressure driven flow based devices operated under the rate of 10 μLmin^{-1} (an equivalent flow rate of that calculated based on the time required to flow 1 mL of serum sample under the given ac-EHD field). Each data point represents the average of three separate trials (n=3) and error bars represent standard error of measurements within each experiment.

presence of a large excess of non-target proteins (10^5 fold higher concentration than target protein) in serum. This detection limit is comparable to that of the traditional bio-barcode[17], immuno-PCR[18], liposome-PCR[19], and redox-cycling[20] based bioassays. Similar detection limits for serum protein detection were also reported using microfluidics[21–23] based platforms. However, their practical application is restricted due to their complex detection procedures, complicated coupling chemistries, pre-concentration/modification steps and operational control systems. Furthermore, current methodologies for removing nonspecific adsorption of non-target serum proteins involves molecular coatings using complicated surface chemistry (*e.g.*, self-assembled monolayers[24], polymer brushes[25,26], polymer based resins[27], etc) coupled with sophisticated detection techniques. In contrast, engendering fluid flow and also shearing off non-target proteins via alternating voltage on asymmetric electrodes-based microfluidic system could be a simple and powerful tool to reduce nonspecific adsorption of proteins and also enhance capture performance of the devices.

In conclusion, we have developed a new method (ac-EHD induced *nanoshearing*) with the capacity to physically dispalce nonspecific adsorption of proteins from solid surfaces. *Nanoshearing* can offer *tuneable* control of surface shear forces and fluid micromixing, which can stimulate fluid flow around the antibody-modified electrodes and can also improve detection of molecular targets due to the increased number of sensor-target interactions. Moreover, since the magnitude of this force can be *tuned* externally, it can be readily adjustable to preferentially select strongly (specifically) bound proteins over more weakly (nonspecifically) bound proteins to surfaces. We have demonstrated the feasibility of using this approach to reduce nonspecific adsorption of proteins by up to 5-fold and also enhance the detection of HER2 protein to as low as 1 fgmL^{-1} in human serum.

Methods

Device design. In this study, we designed two devices containing a combination of planar and/or microtip asymmetric microelectrode pairs within a long microchannel. The device geometry defines the overall characteristic of an electrokinetic system[13,28] The characteristic feature is to maintain the critical gap (r_0) between narrow (d_1) and wide electrodes (d_2) in the pair, which determines the magnitude of the electric field strength. Other parameters including the distance between adjacent electrode pairs (r_1), length of each electrode, and channel dimensions (width (w), height (h) and length (l)) were also considered while designing the devices. We defined the asymmetric electrode pattern with $d_2 > d_1$ and also $r_1 > r_0$. Additionally, the ratio between different length scales of the asymmetric electrode patterns were maintained as follows: $r_0/d_2 = 0.125$, $r_1/d_2 = 0.5$, $d_1/d_2 = 0.25$, where d_2 and d_1 are the lengths of electrodes in the pair, r_0 is the distance between the electrodes in the pair, and r_1 is the distance between adjacent electrode pairs. Unless otherwise stated, all designs were made using Layout Editor (L-edit V15, Tanner research Inc., CA) and written to a photomask. Design of the devices is as follows:

Device 1. A device containing (Supplementary Fig. S1a) 256 asymmetric planar electrode pairs printed on a long serpentine channel (w=400 μm; l=196 mm; h=300 μm) with a 50 μm separation (r_0) between the narrow (d_1=100 μm) and wide electrode (d_2=400 μm). The channels were defined using photolithography by using a polymer coating of negative photoresist (SU8-2150). The channel contains 16 segments connecting each other with 16 electrode pairs in each segment. Adjacent electrode pairs in each segment are separated by a distance of 200 μm (r_1).

Device 2. In order to enhance the fluid micromixing, we incorporated microtips that can create complex flow vortices (*e.g.*, as a result of complex fluid lines) and also provide enhanced surface area due to the increasing device parameters (*e.g.*, length and width of the electrode) along the channel. This device contains 9 asymmetric electrode pairs (Supplementary Fig. S1b) with a combination of planar and microtip electrodes within a long channel (l=22 mm). The electrode dimensions (length × width) increase proportionally along the channel (from electrode pairs 1 to 5), and then decrease towards the outlet (from electrode pairs six to nine). However, similar ratios for r_0/d_2, r_1/d_2 and d_1/d_2 were maintained throughout the channel. Microtips with base diameter of 150 μm were arranged in a square array with a 100 μm distance between two adjacent microtips. The number of microtips remained the same for the first and ninth, second and eighth, third and seventh, fourth and sixth electrode pairs. The fifth electrode pair contains the maximum number of microtips (100 microtips in a 10×10 square array) whilst the first and ninth electrode pairs contained the least number of tips (4 microtips in a 2×2 square array).

Device fabrication and characterization. *Device 1.* Fabrication of **Device 1** is illustrated in Supplementary Fig. S2a. A two-step photolithographic process involves an initial spin coating of a thin film of positive photoresist (AZ1518, Microchem, Newton, CA) onto a Pyrex wafer (thickness, 1 mm). Subsequent UV exposure (150 mJ/cm^2) using a MA6 mask aligner and development (AZ 326MIF developer for 30 s) revealed the patterned electrodes. Metallic layers of Ti (20 nm) and Au (200 nm) were deposited using an electron beam (e-beam) evaporator (Temescal FC-2000) under high vacuum conditions followed by acetone lift-off. The second step includes the construction of a serpentine channel (w=400 μm, h=300 μm) by spin coating (1800 rpm) a negative photoresist (Microchem, SU-8 2150) layer. Subsequently, the wafers were soft baked (65°C for 7 min → 95°C for 60 min → 65°C for 5 min) followed by UV exposure (380 mJ/cm^2). These were then post-baked (65°C for 5 min → 95°C for 20 min → 65°C for 3 min) and developed in propylene glycol methyl ether acetate (PGMEA) for 45 min to reveal the fluidic channel. Individual devices were obtained upon dicing the wafers (ADT 7100 wafer precision dicer), and complete microfluidic devices were obtained upon bonding the devices to glass cover slides containing respective inlet and outlet reservoirs (diameter, 1.5 mm).

Device 2. All process steps involved in the fabrication of **Device 2** are outlined in Supplementary Fig. S2b. Initially, microtips were fabricated using deep reactive ion etching (DRIE). For DRIE, silicon wafers (diameter, 100 mm; thickness, 500 μm; single-side polished) were prepared by spin coating (3500 rpm) a 25 μm layer of negative photoresist (SU-8 2025, Microchem, Newton,CA). Subsequently, the wafers were soft baked (65°C for 3 min → 95°C for 5 min → 65°C for 1 min) and the circular patterns (diameter, 150 μm) were transferred from the photomask onto the wafer upon UV exposure (250 mJ/cm^2). This was followed by a post-baking (from 65°C for 1 min → 95°C for 3 min → 65°C for 1 min) and development step in PGMEA to reveal the circular patterns. Microtips of approximately 85 μm high were obtained using a Plasma therm DRIE etching. A passivation layer of silicon oxide (thickness, 100 nm) was then deposited on the etched wafer using an oxidation furnace. A two-step photolithographic process was performed to fabricate asymmetric gold electrode pairs in a microfluidic channel as outlined for **Device 1**.

All devices were characterized by Scanning Electron Microscopy (SEM) analysis using a JEOL (model 6610) instrument operating at an accelerating voltage of 10 kV.

ac-EHD induced fluid flow visualization. The small and large electrodes within the long channel of the ac-EHD devices (Supplementary Fig. S1a, b) were connected to a signal generator (Agilent 33220A Function Generator, Agilent Technologies, Inc., CA) *via* gold connecting pads and a BNC connector. Fluid flow visualization studies were performed using fluorescent latex particles (Coulter Latron, USA) diluted in PBS (10 mM, pH 7.4). The inlet reservoirs were filled with the particle solutions, and ac field was applied using a signal generator. Fluid flow was monitored using a high speed video camera fitted onto the upright microscope (Nikon Ni-U, Japan).

Device functionalization. The devices were washed with acetone, rinsed with isopropyl alcohol, water and dried with the flow of nitrogen. The array of gold microelectrode pairs within the capture domain of the channel were modified with anti-*HER2* using avidin-biotin chemistry (Supplementary Fig. S5) in a three step process that include: (*i*) incubation with biotinylated BSA (200 μgmL^{-1} in PBS, Invitrogen) solution for 2 h followed by (*ii*) coupling with streptavidin (100 μgmL^{-1} in PBS, Invitrogen) for 1 h at 37°C. (*iii*) streptavidin conjugated channels were coated with biotnylated anti-HER2 (10 μgmL^{-1} in PBS, R&D systems) for another 2 h. Control experiments using serum samples without HER2 included an additional blocking step using 3% BSA for 1 h after anti-HER2 functionalization. Channel was flushed three times with PBS (10 mM, pH 7.4) to remove any unbonded molecules after each step.

HER2 capture and detection. Serum samples were collected from healthy volunteers and upon estimation of total protein using standard Bradford method[29], samples were stored in aliquots (80 μgμl^{-1}) at −80°C. Designated concentration of Human *ErbB2*/HER2 (R&D systems) spiked in PBS or serum was placed in to the inlet reservoirs of the devices and driven through the channel by applying ac-EHD field. The field strength was applied for 30 min with 15 min intervals (without fluid flow) for a total pumping time of 2 h. Control experiments were performed in the absence of ac-EHD field under pressure driven flow conditions using a syringe pump (PHD 2000, Harvard apparatus). Detection antibody FITC conjugated anti-HER2 (2 μgmL^{-1}; R&D systems) and/or Alexafluor 633 anti-IgG (2 μgmL^{-1}; Invitrogen) was driven through the channel under ac-EHD and/or pressure driven flow conditions. Devices were washed repeatedly in PBS and imaged under a fluorescence microscope (Nikon eclipse Ni-U upright microscope). Image analysis was performed using the image processing software (Nikon Ni-S elements, Basic Research) by considering a region of interest to obtain a count of the fluorescence spots based on fluorescence intensity range, size and circularity. The intensity range for the particular wavelength (*e.g.*, FITC, AlexaFluor) was set based on the mean intensity. The length scale chosen was set to scan spots < 1 μm during the analysis. For comprehensive and improved data analysis, images were captured on similar electrode pairs for each device during individual trials and the 400 μm × 400 μm region of interest was maintained.

1. Houseman, B. T. & Mrksich, M. Towards quantitative assays with peptide chips: a surface engineering approach. *Trends Biotechnol.* **20**, 279–281 (2002).

2. Shim, M., Kim, N. W. S., Chen, R. J., Li, Y. & Dai, H. Functionalization of Carbon Nanotubes for Biocompatibility and Biomolecular Recognition. *Nano. Lett.* **2**, 285–288 (2002).
3. Shiddiky, M. J. A., Kithva, P. H., Rauf, S. & Trau, M. Femtomolar detection of a cancer biomarker protein in serum with ultralow background current by anodic stripping voltammetry. *Chem. Commun.* **48**, 6411–6413 (2012).
4. Grewal, Y. S. *et al.* Label-free electrochemical detection of an *Entamoeba histolytica* antigen using cell-free yeast-scFv probes. *Chem. Commun.* **49**, 1551–1553 (2013).
5. Cooper, S. L. & Peppas, N. A. *Biomaterials: Interfacial phenomena and applications.* (American Chemical Society, Washington, 1982).
6. Chambers, L. D., Stokes, K. R., Walsh, F. C. & Wood, R. J. K. Modern approaches to marine antifouling coatings. *Surf. Coat. Technol.* **201**, 3642–3652 (2001).
7. Ostuni, E., Chen, C. S., Ingber, D. E. & Whitesides, G. M. Selective Deposition of Proteins and Cells in Arrays of Microwells. *Langmuir* **17**, 2828–2834 (2001).
8. Banerjee, I., Pangule, R. C. & Kane, R. S. Antifouling coatings: recent developments in the design of surfaces that prevent fouling by proteins, bacteria, and marine organisms. *Adv. Mat.* **23**, 690–718 (2011).
9. Nelson, K. E., Foley, J. O. & Yager, P. Concentration Gradient Immunoassay. 1. An Immunoassay Based on Interdiffusion and Surface Binding in a Microchannel. *Anal. Chem.* **79**, 3542–3548 (2007).
10. Sung Kim, K. & Park, J-K. Magnetic force-based multiplexed immunoassay using superparamagnetic nanoparticles in microfluidic channel. *Lab Chip* **5**, 657–664 (2005).
11. Brown, A. B. D., Smith, C. G. & Rennie, A. R. Pumping of water with ac electric fields applied to asymmetric pairs of microelectrodes. *Phys. Rev. E* **63**, 016305 (2000).
12. Ramos, A., González, A., Castellanos, A., Green, N. G. & Morgan, H. Pumping of liquids with ac voltages applied to asymmetric pairs of microelectrodes. *Phys. Rev. E* **67**, 056302 (2003).
13. Hunter, R. J. *Foundations of colloidal science*, (Oxford University Press Inc., New York, 1987).
14. Green, N. G., Ramos, A., González, A., Morgan, H. & Castellanos, A. Fluid flow induced by nonuniform ac electric fields in electrolytes on microelectrodes. I. Experimental measurements. *Phys. Rev. E* **61**, 4011 (2000).
15. Yeh, S., Seul, M. & Shraiman, B. I. Assembly of ordered colloidal aggregates by electric field induced fluid flow. *Nature* **386**, 57 (1997).
16. Trau, M., Saville, D. A. & Aksay, I. A. Assembly of colloidal crystals at electrode interfaces. *Langmuir* **13**, 6375–6381 (1997).
17. Nam, J. M., Thaxton, C. S. & Mirkin, C. A. Nanoparticle-based bio-bar codes for the ultrasensitive detection of proteins. *Science* **26**, 1884–86 (2003).
18. Niemeyer, C. M., Adler, M. & Wacker, R. Immuno-PCR: high sensitivity detection of proteins by nucleic acid amplification. *Trends Biotechnol.* **23**, 208–216 (2005).
19. Mason, J. T., Xu, L., Sheng, Z-M. & O'Leary, T. J. A liposome-PCR assay for the ultrasensitive detection of biological toxins. *Nat. Biotechnol.* **24**, 555–557 (2006).
20. Das, J., Aziz, M. A. & Yang, H. A Nanocatalyst-based assay for proteins: DNA-free ultrasensitive electrochemical detection using catalytic reduction of *p*-nitrophenol by gold-nanoparticle labels. *J. Am. Chem. Soc.* **128**, 16022–16023 (2006).
21. Yan, J. *et al.* A Nano- and micro- integrated protein chip based on quantum dot probes and a microfluidic network. *Nano Res.* **1**, 490–96 (2008).
22. Hu, M. *et al.* Ultrsensitive, multiplexed detection of cancer biomarkers directly in serum by using quantum-dot based microfluidic protein chip. *ACS Nano.* **4**, 488–94 (2009).
23. Tekin, H. C. & Gijs, M. A. M. Ultrasenstive protein detection: a case for microfluidic magnetic bead-based assays. *Lab Chip.* **13**, 4711–39 (2013).
24. Ladd, J., Zhang, Z., Chen, S., Hower, J. C. & Jiang, S. Zwitterionic Polymers Exhibiting High Resistance to Nonspecific Protein Adsorption from Human Serum and Plasma. *Biomacromolecules* **9**, 1357–61 (2008).
25. Heuberger, R., Sukhorukov, G., Voros, J., Textor, M. & Mohwald, H. Biofunctional Polyelectrolyte Multilayers and Microcapsules: Control of Non-specific and Bio-specific Protein Adsorption. *Adv. Func. Mat.* **15**, 357–66 (2005).
26. Hucknall, A., Rangarajan, S. & Chilkot, A. In Pursuit of Zero: Polymer Brushes that Resist the Adsorption of Proteins. *Adv. Mat.* **21**, 2441–46 (2009).
27. Tamura, T., Terada, T. & Tanaka, A. A Quantitative Analysis and Chemical Approach for the Reduction of Nonspecific Binding Proteins on Affinity Resins. *Bioconjugate Chem.* **14**, 1222–30 (2003).
28. Olesen, L. H., Bruus, H. & Ajdari, A. Ac electrokinetic micropumps: the effect of geometrical confinement, Faradaic current injection, and nonlinear surface capacitance. *Phys Rev E.* **73**, 056313 (2006).
29. Kruger, N. J. *The Protein Protocols Handbook.* (Spinger protocols, 2009).

Acknowledgments

This work was supported by the ARC DECRA (DE120102503) to MJAS. We also acknowledge funding received by our laboratory from the National Breast Cancer Foundation of Australia (CG-08-07 and CG-12-07) to MT. These grants have significantly contributed to the environment to stimulate the research described here. The device fabrication was performed at Queensland node of the Australian National Fabrication Facility (Q-ANFF).

Author contributions

M.J.A.S. and M.T. conceived the idea and supervised the project. M.J.A.S., M.T. and R.V. designed the experiments, R.V. and Z.T. conducted most experiments, S.R. helped with device design and fabrication. All authors discussed the results and wrote the manuscript.

Additional information

Supplementary information accompanies this paper at http://www.nature.com/scientificreports

Competing financial interests: The authors declare no competing financial interests.

How to cite this article: Shiddiky, M.J.A., Vaidyanathan, R., Rauf, S., Tay, Z. & Trau, M. Molecular *Nanoshearing*: An Innovative Approach to Shear off Molecules with AC-Induced Nanoscopic Fluid Flow. *Sci. Rep.* **4**, 3716; DOI:10.1038/srep03716 (2014).